International Journal of Natural and Engineering Sciences
E-ISSN: 2146-0086 15(1): 17-34, 2021
Research Article

DIRECT ACTIVE AND REACTIVE POWERS COMMAND WITH THIRD-ORDER SLIDING MODE THEORY FOR DFIG-BASED DUAL-ROTOR WIND POWER SYSTEMS

Benbouhenni Habib [1,a,*]

[1]*Nişantaşı University, İstanbul, Turkey*

**Corresponding Author:*
E-mail: habib0264@gmail.com

(Received 15th March 2021; accepted 21th March 2021)

a: ORCID 0000-0001-8253-4863

ABSTRACT. In this paper, we present a novel nonlinear method using proposed third-order sliding mode command (TOSMC) for the doubly-fed induction generator (DFIG) controlled by direct reactive and active powers command (DRAPC). In the first place, we establish the proposed mathematical models of the proposed TOSMC controller. To regulate the power flowing between the grid and the DFIG, a proposed strategy design uses the proposed TOSMC method is applied for implementing to minimize the torque ripple, reactive and active powers oscillations on a traditional DRAPC method. The use of this controller provides very satisfactory effectiveness for the DFIG command, and the chattering effect is also more minimized by this proposed controller. The proposed TOSMC controllers which are insensitive to uncertainties, including parameter modification and external disturbances in the whole command process. Finally, the DRAPC with proposed TOSMC controllers is used to regulate the reactive and active powers of a DFIG-based dual-rotor wind turbine (DRWT) and confirms the validity of the proposed controllers. Results of simulations containing tests of tracking and robustness tests are presented.

Keywords: *Doubly fed induction generator, third-order sliding mode command, dual rotor wind turbine, direct reactive and active powers command*

INTRODUCTION

Traditionally, sliding mode controller (SMC) was based on the technique of nonlinear control, since the durability, solidity, simplicity and robustness are the advantages of the SMC controllers. The SMC controller has attracted a lot of work on nonlinear control theory in recent years. The SMC controller was originally introduced in the 1977s by Utkin. Its application has been in electrical engineering, electronic and automatic. In [1], the authors designed the use of a direct reactive and active powers command (DRAPC) with SMC controllers applied to the DFIG-based wind turbine. An SMC controller was designed to minimize the reactive and active powers of the DFIG [2]. In [3], an integral SMC controller was designed to control the active power and torque. The principal drawbacks of the SMC controller is that the chattering phenomenon. To resolve this problem, many works have been proposed to reduce the chattering phenomenon. In [4], a modified SMC method was proposed based on a neural algorithm, where a sign controller of SMC was replaced by neural methods. In [5], the electromagnetic torque ripple is reduced by using the fuzzy SMC controller. SMC controller and neuro-fuzzy algorithm are combined to reduce the reactive and active powers of the DFIG [6].

For high performance SMC controller, a second-order SMC (SOSMC) was proposed in the works [7-12]. It is a simple method, robust strategy, and easy to implement. It can offer many good specifications such as insensitivity to parameters variation, good

performances against unmodeled dynamics, and fast dynamic response. A fuzzy SOSMC technique was designed to minimize the harmonic distortion (THD) of the current [13]. SOSMC and neuro-fuzzy algorithm are composite to minimize the torque ripple, reactive and active powers oscillations relative to traditional SOSMC method of the DFIG. In [14], the authors designed the use of a direct field-oriented command with super-twisting SMC (STSM) algorithms applied to the six-phase induction motor drive. The STSM algorithm is a type of SOSMC controller. The advantage of an STSM controller is a robust method and simple strategy. STSM control is one of the most used robust control techniques for AC machine drives. This method was introduced in the 1999s by Utkin *et al*. its principle is based on a modification of the traditional proportional-integral (PI) controller. In [15], the authors proposed the use of a DRAPC method with neuro-fuzzy STSM controllers applied to the DFIG. A direct torque and flux control (DTFC) was proposed based on STSM controllers, where the traditional PI controllers were replaced by STSM algorithms [16]. This proposed DTFC is a simple algorithm and reduced the THD value of current compared to the traditional DTFC method. In [17], the DTFC method based on the neural STSM technique has been designed. However, the neural STSM controller is a modified of the STSM controller, where the Sgn(U) is replaced by neural algorithm. In [18], a modified STSM controller was proposed based on the fuzzy logic controller to obtain high-performance DTFC method of the DFIG-based wind turbine. In [19], torque and rotor flux neuro-fuzzy STSM controllers and modified space vector modulation (MSVM) were united to replace the hysteresis controllers and classical lookup table.

In this work direct active and reactive powers control scheme of the DFIG integrated to DRWT systems with proposed TOSMC controllers is presented. Theoretical principles of the proposed TOSMC controller are presented along with simulation results. Specifications of the DRAPC with the application of proposed TOSMC controllers over the classical DRAPC strategies presented. The main advantages of the DRAPC-TOSMC control scheme are its good dynamic response, robust technique, simple algorithm, and constant switching frequency operation. This work compares classical DRAPC with a hysteresis controllers and proposed DRAPC with proposed TOSMC controllers applied to DFIG-based DRWT systems. Analysis of the DRAPC with the application of the designed TOSMC controllers has been done in MATLAB software. Simulation results are presented. The THD value of stator current are more reduced when proposed TOSMC controllers is used.

THIRD ORDER SLIDING MODE CONTROL

The proposed third-order SMC controller is based on the design of the discontinuous command signal that drives the system states toward special manifolds in state space. The proposed TOSMC technique is designed to minimize the chattering phenomenon. This proposed technique is based on the classical STSM controller. The proposed TOSMC technique solves the problem of minimizing a power ripple of the DFIG, a very fast method, simple algorithm, and robust strategy. The command law of the proposed TOSMC controller can be defined as follows:

$$\begin{cases} u = K_1 |S|^r \, sat(S) + K_2 \, sat(S) + u_1 \\ \dfrac{d\,u_1}{dt} = K_3 \, sat(S) \end{cases} \quad (1)$$

where *s* is the switching function determined for the proposed TOSMC controller. K_1, K_2, and K_3 are the coefficients of the proposed TOSMC controller. R is the exponent defined for the proposed TOSMC controller.

The structure of the command law of the proposed TOSMC technique is shown in Fig. 1.

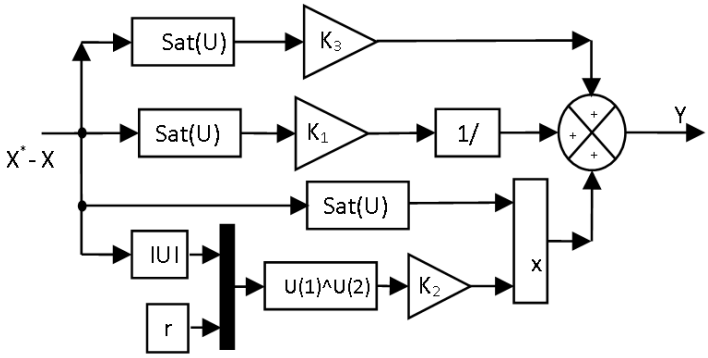

Fig. 1. *Structure of the command law of the proposed TOSMC controller*

The value of the exponent *r* has an impact on the dynamics of the command technique with proposed TOSMC strategy. This exponent can have a value between zero and one. The stability of the TOSMC controller is proven using the Lyapunov technique.

The proposed TOSMC controller preserves the advantages of the classical STSM algorithm such as fast response dynamic, simplicity, and robustness method. Also, the mathematical model of the system is not needed.

The procedure for determining the coefficients K1, K2 and K3 of the proposed TOSMC controllers is based on the analysis of equations for the nonlinear command system and the output signals. These equations in the matrix are presented as follows:

$$\begin{cases} \dfrac{d^2x}{dt^2} = a(x,t) + b(x,t)u + c(x,t)\dfrac{du}{dt} \\ y = d(x,t) \end{cases} \tag{2}$$

where y is the vector of output control signals; u is the vector of input control signals; x is the state vector of the system; a(x, t), b(x, t), c(x, t) and d(x, t) are the vector functions.

The third time derivative of equations for the output signals has the matrix form presented as follows:

$$\frac{d^3y}{dt^3} = A(x,t) + B(x,t)\frac{dy}{dt} + C(x,t)\frac{d^2y}{dt^2} \tag{3}$$

The bounds of A(x, t), B(x, t) and C(x, t) of the third derivative of y can be labelled as A_M, A_m, B_M, B_m, C_M and C_m, where A_M, B_M and C_M are upper bounds and A_m B_m and C_m are lower bounds. The K_1, K_2 and K_3 are determined for all TOSMC controller according to the equations presented as follows:

$$K_1 > \frac{A_M + B_M}{C_m},\ K_2 \geq \frac{4(A_M + B_M)}{{C_m}^3} \cdot \frac{C_M(K_1 + C_M)}{B_m(K_1 - C_M)} \tag{4}$$

DRWT SYSTEM

The DRWT system is a wind turbine for solving both problems that are based on a single rotor wind turbines (SRWTs). The DRWT uses two wind turbine rotating in opposite directions on the same axis. However, the SRWT system is the most common wind turbine used in the generates electrical power. The mathematical model of the DRWT system is different from the SRWT system. The DRWT system has been designed as new wind power, as shown in Fig. 2. The DRWT system gives more power coefficient and aerodynamic torque compared to the SRWT system. The DRWT system design is composed of two wind turbines, the main turbine and the auxiliary turbine [20]. The control of the DRWT system is difficult compared to the SRWT system. The total aerodynamic power of the DRWT system is the auxiliary turbine power (P_A) add to the main turbine power (P_M) as shown by the following equation:

$$P_{DRWT} = P_T = P_M + P_A \quad (5)$$

Where: P_M: Main turbine power.
P_A: auxiliary turbine power.
P_T: total aerodynamic power.

The total torque of the DRWT system is given:

$$T_T = T_M + T_A \quad (6)$$

Where: T_M: Main turbine torque.
T_A: Auxiliary turbine torque.
T_T: Total aerodynamic torque.

The aerodynamic torque of the auxiliary turbine is given [21]:

$$T_A = \frac{1}{2\lambda_A^3}.\rho.\pi.R_A^5.C_p.w_A^2 \quad (7)$$

The aerodynamic torque of the main turbine is given:

$$T_M = \frac{1}{2\lambda_M^3}.\rho.\pi.R_A^5.C_p.w_M^2 \quad (8)$$

With R_A, R_M: Blade radius of the main and auxiliary turbines, λ_A, λ_M: the tip speed ration of the main and auxiliary turbines, ρ: the air density and w_M, w_A the mechanical speed of the main and auxiliary turbines.

The tip speed ratios of the auxiliary turbine is given:

$$\lambda_A = \frac{w_A.R_A}{V_1} \quad (9)$$

The tip speed ratios of the main turbine is given:

$$\lambda_M = \frac{w_M.R_M}{V_M} \quad (10)$$

Where V_M is the speed of the unified wind on main turbine and V_1 is the wind speed on an auxiliary turbine. Obtaining the wind speed on the auxiliary turbine is straight forward. However, calculation of wind speed on the main turbine requires further

investigation. Based on the (11), it is possible to estimate the amount of the wind speed at any point between the main and auxiliary blades.

$$V_x = V_1(1-\frac{1-\sqrt{(1-C_T)}}{2}(1+\frac{2.x}{\sqrt{1+4.x^2}})) \tag{11}$$

With C_T the trust coefficient, which is taken to be 0.9, and x is the non-dimensional distance from the auxiliary rotor disk, Vx the velocity of the disturbed wind between rotors at point x. So, with respect to x=15, the value of the Vx close to the main rotor is computable (rotors are located 15 meters apart from each other) [22].

The power coefficient is given:

$$C_p(\lambda,\beta) = 0.517(\frac{116}{\lambda_i} - 0.4\beta - 5)e^{-\frac{21}{\lambda_i}} + 0.0068\lambda \tag{12}$$

$$\frac{1}{\lambda_i} = \frac{1}{\lambda + 0.08\beta} - \frac{0.035}{\beta^3 + 1} \tag{13}$$

With β is pitch angle.

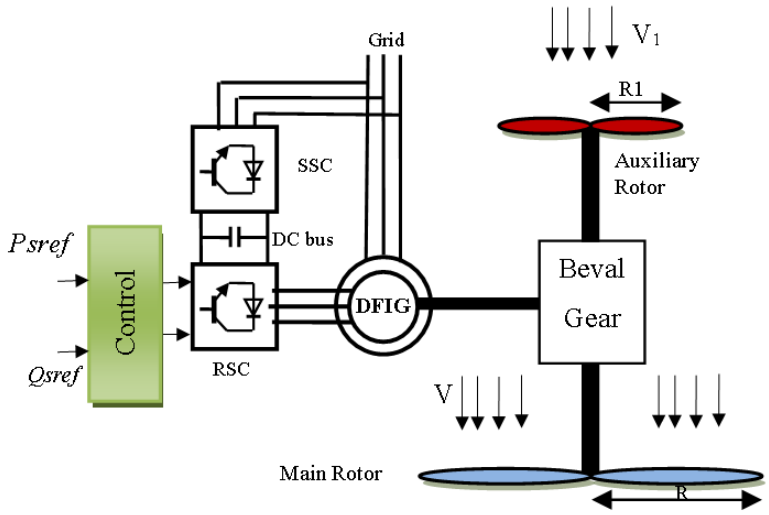

Fig. 2. *Structure of DRWT with a DFIG*

DRAPC CONTROL SCHEME

In the classical DRAPC control, two traditional hysteresis comparators are used to control the reactive and active powers. The main the advantage of DRAPC strategy is the using of a lookup table that minimizes electromagnetic torque ripple, reactive and active powers of the DFIG compared to field-oriented command. Moreover, the DRAPC method with a lookup table is robust control, a simple algorithm, and gives small harmonic components. Nowadays, high attention to DRAPC methods leads to novel algorithms with a wide diversity of techniques [23]. Neural DRAPC strategy, fuzzy DRAPC control, robust DRAPC strategy, neuro-fuzzy DRAPC strategy and DRAPC

with SVM technique are five basic techniques of DRAPC strategy. To regulate the active and reactive powers to the desired values, DRAPC control uses the generator models to predict the voltage required. To estimate the instantaneous reactive and active powers, we use only voltage and current measurements. In this method, the three-level hysteresis controllers are used to regulate the active power and two-level hysteresis controllers are used to regulate the reactive power. Also, the lookup table is used to engender in the output voltages and or currents phases applied to rotor DFIG less THD value and to provide more efficiency.

The classical DRAPC objective is to regulate the active and stator reactive power of the DFIG. In the DRAPC strategy, active power is regulated by the quadrature axis voltage Vqr, while the stator reactive power is regulated by the direct axis voltage Vdr. The classical DRAPC technique, which is proposed to regulate the reactive and active powers of the DFIG-based DRWT systems, is shown in Figure 3.

The estimated reactive and active powers as in Eqs. (14) and (15) [24].

$$Q_s = -\frac{3}{2}\left(\frac{V_s}{\sigma.L_s}\cdot\varphi_{r\beta} - \frac{V_s.L_m}{\sigma.L_s.L_r}\cdot\varphi_{r\alpha}\right) \tag{14}$$

$$P_s = -\frac{3}{2}\frac{L_m}{\sigma.L_s.L_r}\cdot(V_s.\varphi_{r\beta}) \tag{15}$$

Where:

$$\Psi_{s\beta} = \sigma L_r I_{r\beta} \tag{16}$$

$$\Psi_{s\alpha} = \sigma L_r I_{r\alpha} + \frac{M}{L_s}\Psi_s \tag{17}$$

$$\sigma = 1 - \frac{M^2}{L_r L_s} \tag{18}$$

The DRAPC lookup table is as shown in Table 1.

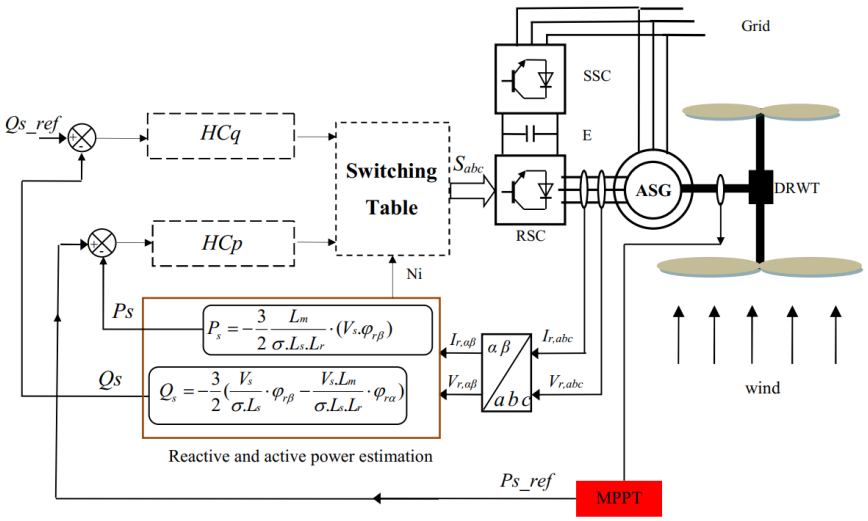

Fig. 3. *DRAPC system of DFIG-based DRWT system*

Table 1. *Switching table for DRAPC strategy*

N		**1**	**2**	**3**	**4**	**5**	**6**
Hq	**Hp**						
1	**1**	5	6	1	2	3	4
	0	7	0	7	0	7	0
	-1	3	4	5	6	1	2
0	**1**	6	1	2	3	4	5
	0	0	7	0	7	0	7
	-1	2	3	4	5	6	1

TOSMC-DRAPC STRATEGY

The DRAPC strategy of the DFIG-based DRWT system with the application of the proposed TOSMC controllers is shown in Fig. 4. In this designed technique, the reactive and active powers are regulated by the proposed TOSMC methods. However, the proposed DRAPC strategy is a robust method, easy and simple algorithms. Besides, the DRAPC control with proposed TOSMC controllers minimized the THD value of stator voltage, active and reactive powers oscillations compared to traditional DRAPC strategy.

In the outer command loop of the active power, the reference value of the active power is compared with the measured active power. The sliding surface for active power regulator can be specified as follows :

$$S_{PS} = P_S^* - P_S \tag{19}$$

The controller of the active power determines the reference Vqr component of rotor voltage vector, which is responsible for the command of DFIG active power. The output signal for the active power regulator is fixed by the following system of equations:

$$\begin{cases} V_{qr}^* = K_{1Ps}\left|S_{PS}\right|^r sat(S_{PS}) + K_{2Ps} sat(S_{PS}) + V_{qr1}^* \\ \dfrac{dV_{qr1}^*}{dt} = K_{3Ps} sat(S_{PS}) \end{cases} \tag{20}$$

Where K_{1Ps}, K_{2Ps} and K_{3Ps} are the coefficients of the TOSMC active power regulator.

In the outer command loop of the reactive power, the reference value of the reactive power is compared with the measured reactive power. The surface for reactive power regulator can be specified as follows:

$$S_{QS} = Q_S^* - Q_S \tag{21}$$

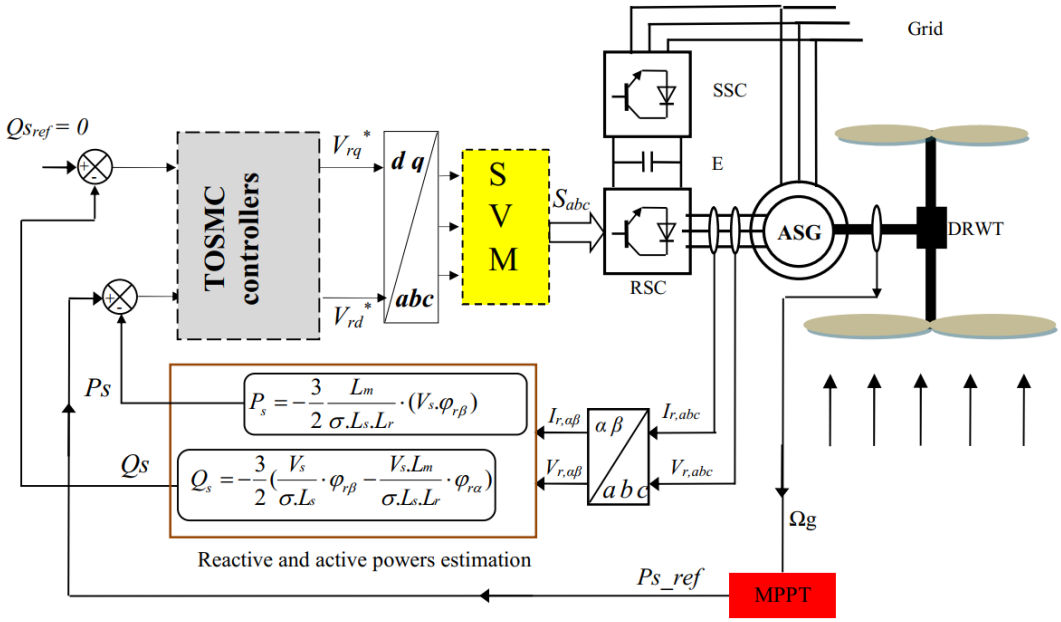

Fig. 4. *DRAPC system of DFIG with the applications of proposed TOSMC controllers.*

The controller of the reactive power determines the reference Vdr component of rotor voltage vector, which is responsible for the command of DFIG reactive power. The output signal for the reactive power regulator is determined by the following system of equations:

$$\begin{cases} V_{dr}^{*} = K_{1Qs}\left|SQ_s\right|^{r} sat(SQ_s) + K_{2Qs}\, sat(SQ_s) + V_{dr1}^{*} \\ \dfrac{dV_{dr1}^{*}}{dt} = K_{3Qs}\, sat(SQ_s) \end{cases} \tag{22}$$

Where K_{1Qs}, K_{2Qs} and K_{3Qs} are the coefficients of the TOSMC reactive power regulator.

The proposed TOSMC controller of the active power is shown in Fig. 5.

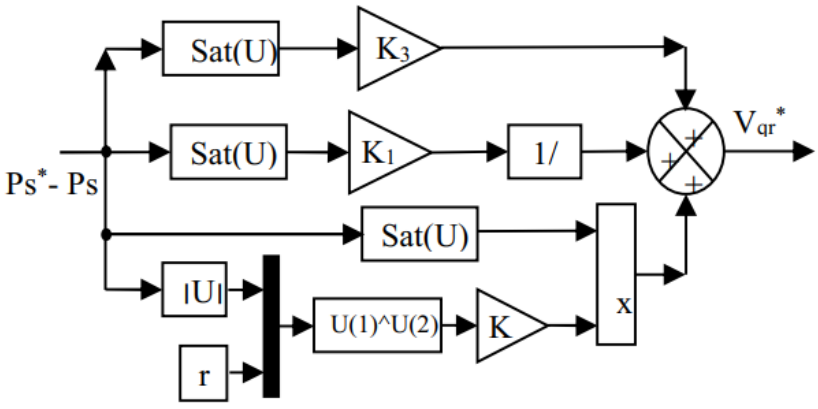

Fig. 5. *Structure of the designed TOSMC active power regulator.*

The proposed TOSMC regulator of the reactive power is shown in Fig. 6.

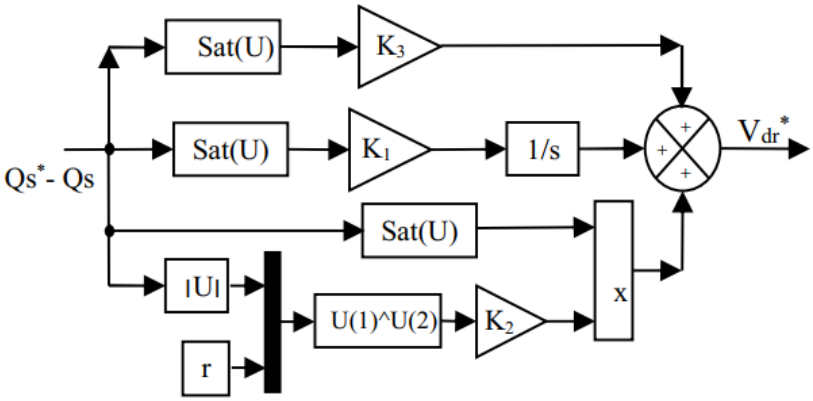

Fig. 6. *Structure of the designed TOSMC reactive power regulator.*

RESULTS AND ANALYSIS

The simulation results of the DRAPC strategy with proposed TOSMC regulators of the DFIG-based DRWT system are compared with the classical DRAPC technique. The simulations were implemented with Matlab software package for a step of sampling time T= $1x10^{-5}$s.

The DFIG parameters are: stator voltage : 380/696V, two poles, P_{sn}=1.5 MW, 50Hz; R_s = 0.012 Ω, J = 1000 kg.m^2, R_r = 0.021 Ω, L_r = 0.0136H, L_s = 0.0137H, L_m = 0.0135H, and f_r = 0.0024 Nm/s [25].

1.

A. Reference tracking test

The simulation waveforms of the measured and reference active power of the DFIG-based DRWT system are shown in Fig. 7 in order to compare the effectiveness of the DRAPC technique with the application of the proposed TOSM controllers with the effectiveness of the classical DRAPC technique with application of the lookup table. It can be stated that during the start-up for the DRAPC strategy with the proposed TOSMC controllers, the active and follows the reference active power faster than for the structure with a lookup table.

The simulation result of the reactive power of DFIG for DRAPC strategy with the application of proposed TOSMC controllers and classical DRAPC strategy is shown in Fig. 8. At the load condition, the reactive power becomes identical as the reactive power reference.

The simulation waveforms of the torque of the DFIG For the proposed strategies are shown in Fig. 9 to compare the effectiveness of the DRAPC strategy with the application of the proposed TOSMC controllers with the effectiveness of the classical DRAPC with the application of the lookup table. The amplitudes of the electromagnetic torque depend on the value of the load active power.

The simulation waveforms of the stator current (Ias) of the classical DRAPC and DRAPC with proposed TOSMC controllers are shown in Fig. 10. These waveforms demonstrate that the analyzed DRAPC with proposed TOSMC controllers allows to obtaining command signals with the waveforms similar to the output signals from classical DRAPC strategy. The amplitudes of the currents depend on the state of the drive system and the value of the load reactive and active powers.

Figs. 11-12 show the THD value of current (Ias) of the DFIG for classical DRAPC and DRAPC with proposed TOSMC controllers respectively. It can be seed that the THD value is minimized DRAPC with proposed TOSMC controllers (0.23%) when compared to classical DRAPC strategy (0.40%).

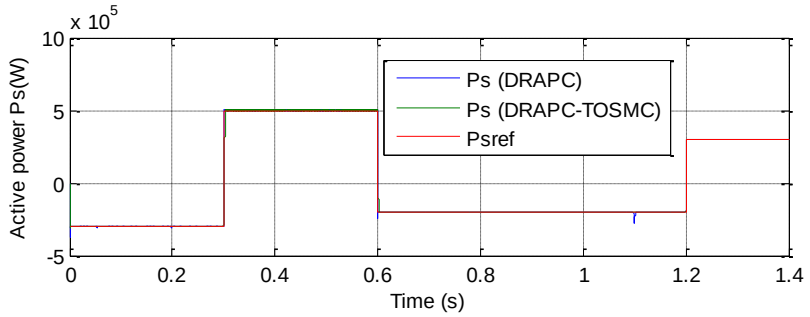

Fig. 7. *Active power.*

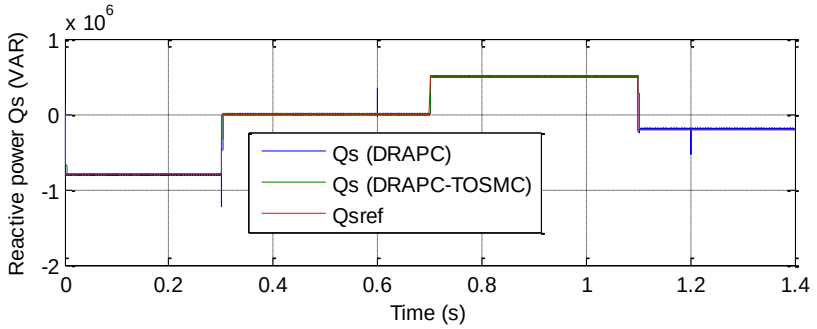

Fig. 8. *Reactive power.*

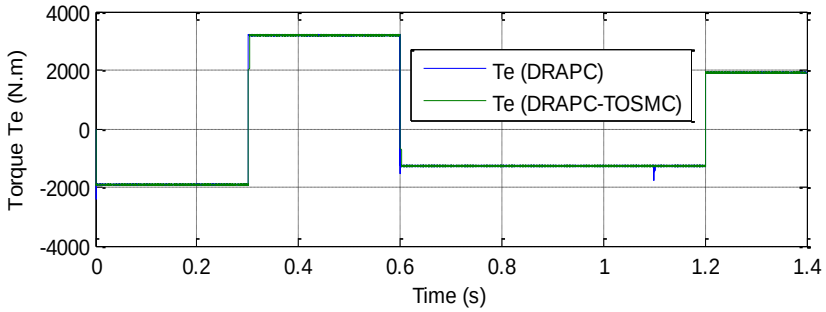

Fig. 9. *Torque.*

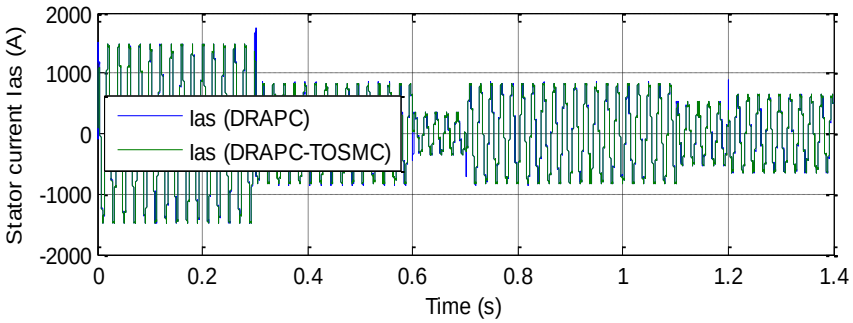

Fig. 10. *Current.*

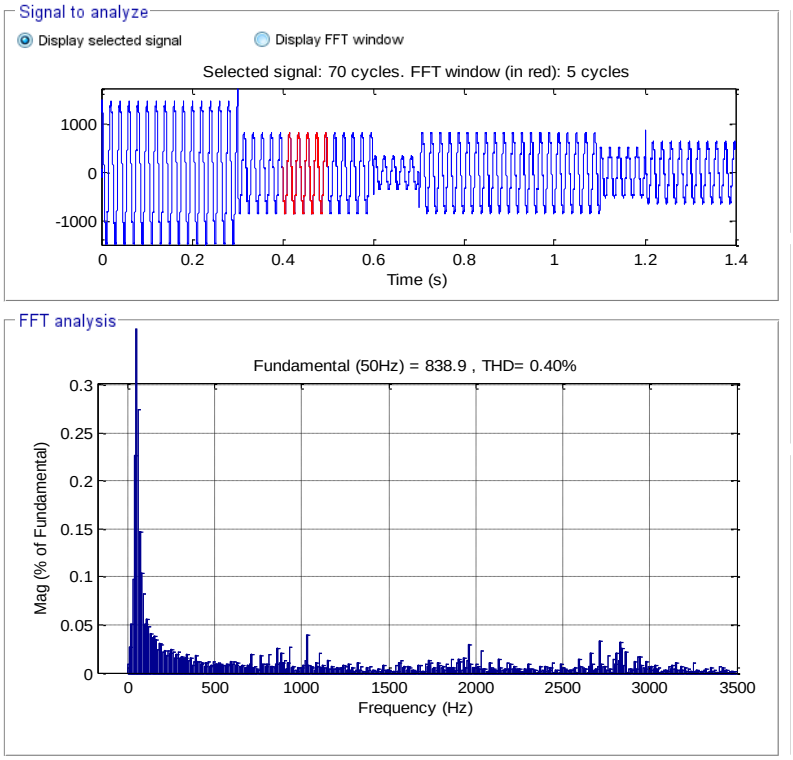

Fig. 11. *THD (DRAPC strategy).*

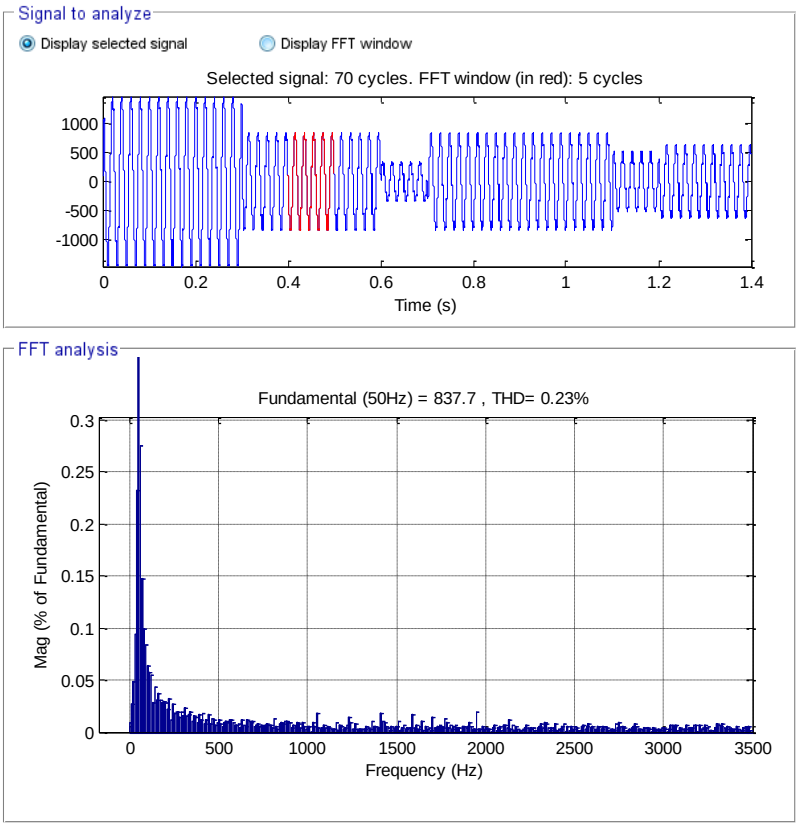

Fig. 12. *THD (TOSMC-DRAPC strategy).*

The zoom in the active power, reactive power, electromagnetic torque and stator current is shown in Figs. 13-15, and Fig. 1, respectively. It can be seen that the DRAPC control with proposed TOSMC controllers reduced the ripples in reactive power, active power, torque and current compared to the classical DRAPC strategy.

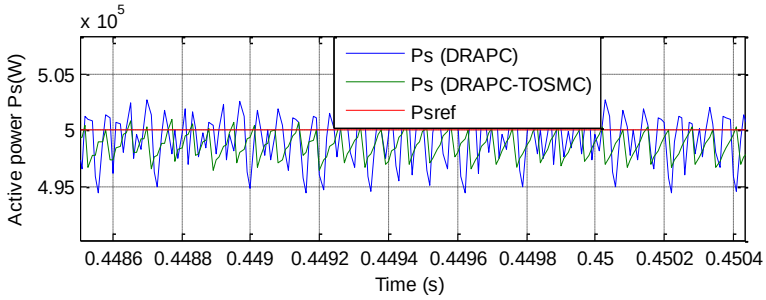

Fig. 13. *Zoom (Active power).*

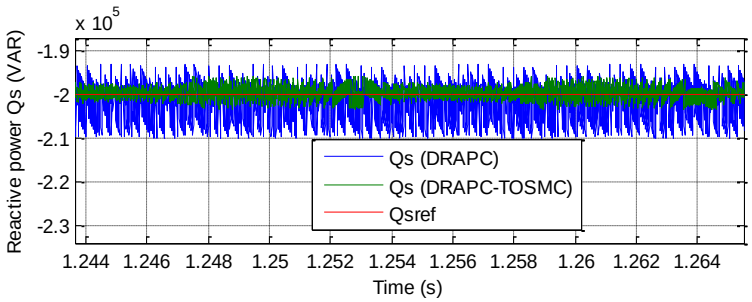

Fig. 14. *Zoom (Reactive power).*

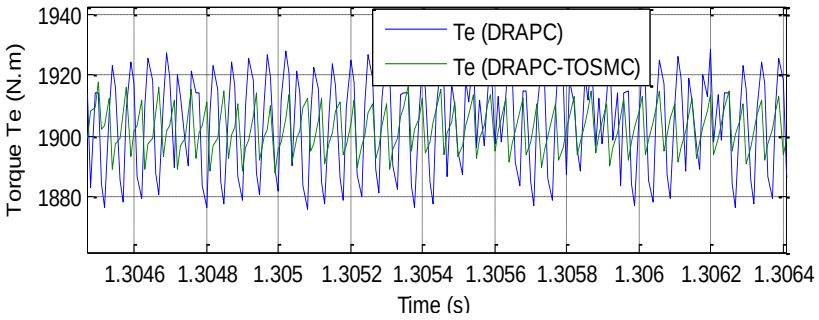

Fig. 15. *Zoom (Torque).*

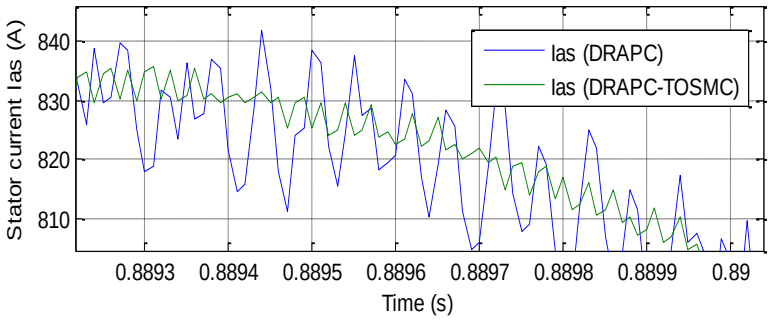

Fig. 16. *Zoom (Current).*

B. Robustness test

In this part, the nominal value of inductances L_s, M, and L_r are halfed and the value of R_r and R_s is doubled, Simulation results are presented in Figures 17-22. The simulation waveform of the reactive and active powers of DFIG for proposed DRAPC strategies is shown in Figs. 17 and 18, respectively. At the load condition, the active and reactive powers become identical as the load active and reactive powers. The simulation waveforms of the torque of the DFIG-based DRWT system are shown in Fig. 19. It can be stated that the value of the electromagnetic torque of DRAPC with proposed TOSMC controllers is equal to the value of the electromagnetic torque of classical DRAPC with a lookup table. The simulation waveforms of all Ias of DFIG for the proposed DRAPC strategies are shown in Fig. 20. It can be stated that the value of the Ias of DRAPC with proposed TOSMC controllers is equal to the value of the Ias of classical DRAPC with a lookup table. The THD value of the Ias in the DRAPC with proposed TOSMC controllers has been significantly minimized. Thus it can be concluded that the DRAPC with proposed TOSMC controllers is more robust than the DRAPC with a lookup table.

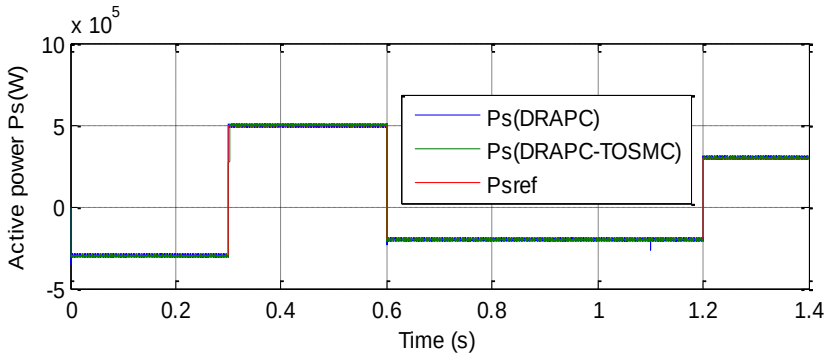

Fig. 17. *Active power.*

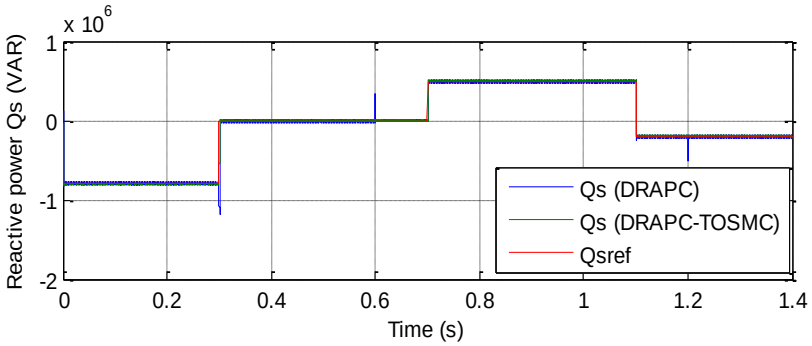

Fig. 18. *Reactive power.*

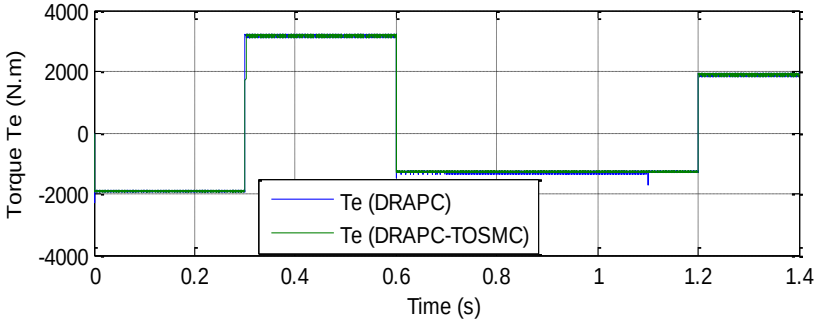

Fig. 19. *Torque.*

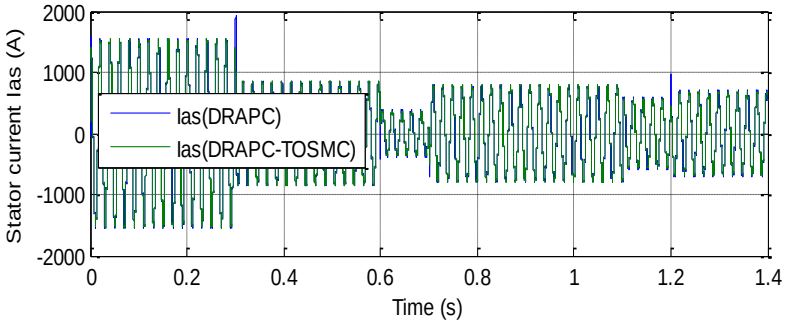

Fig. 20. *Current.*

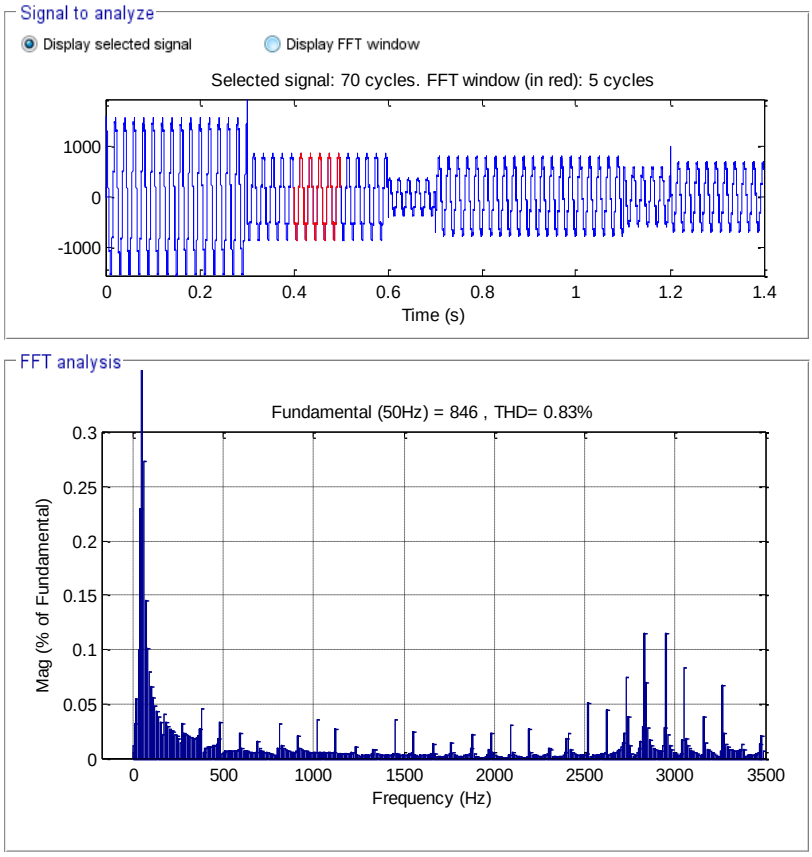

Fig. 21. *THD (DRAPC strategy).*

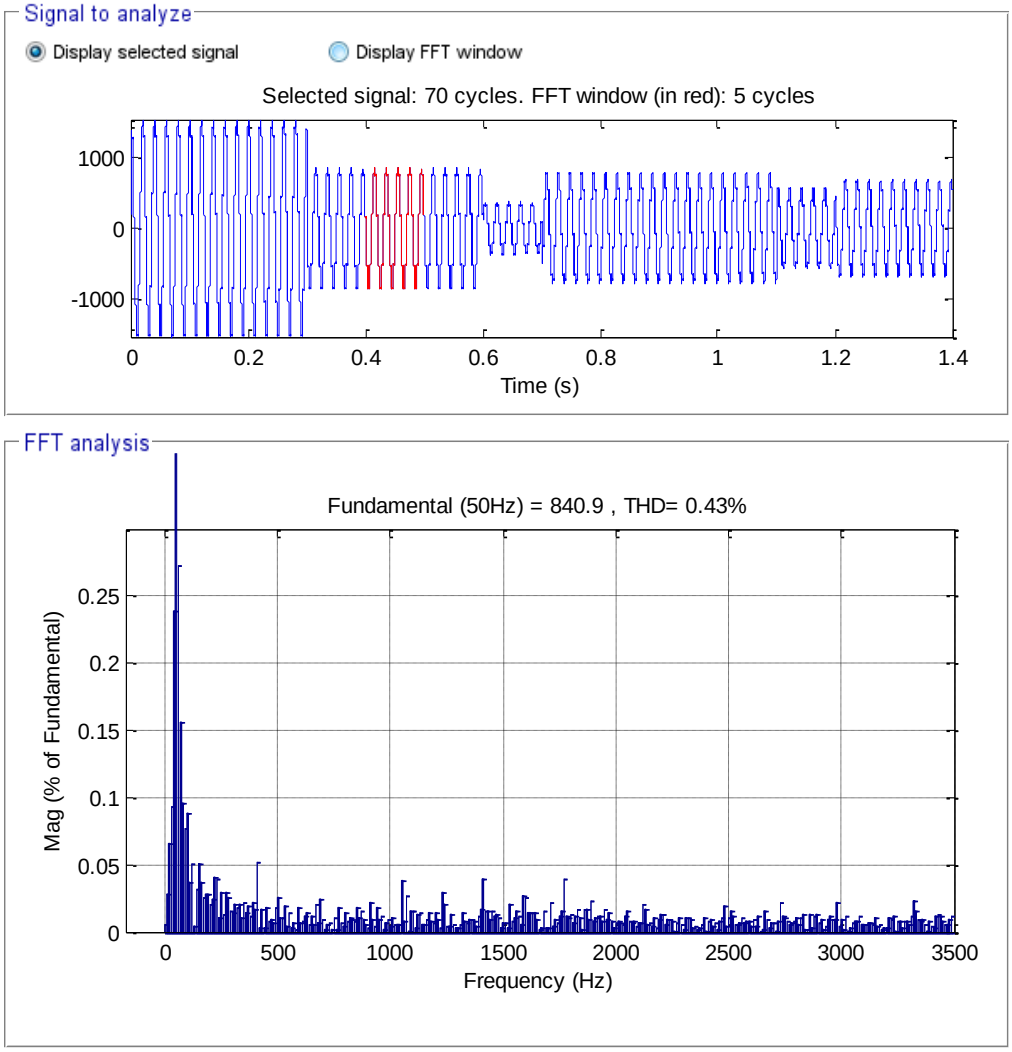

Fig. 22. *THD (TOSMC-DRAPC strategy).*

The zoom in the active/reactive power, electromagnetic torque and current is shown in Figs. 23-26, respectively. It can be clearly observed that the DRAPC control with proposed TOSMC controllers minimized the ripples in reactive power, active power, torque and current compared to the classical DRAPC strategy.

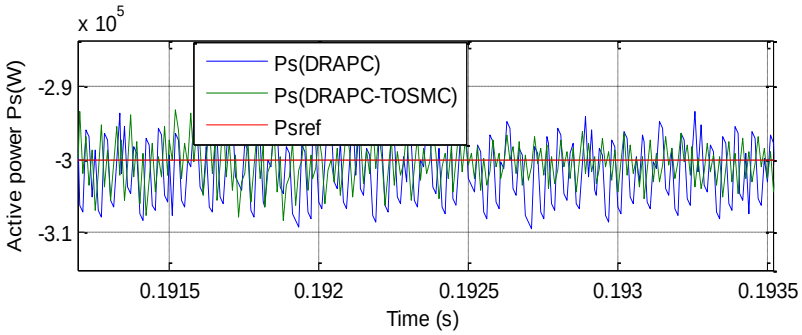

Fig. 23. *Zoom in the active power.*

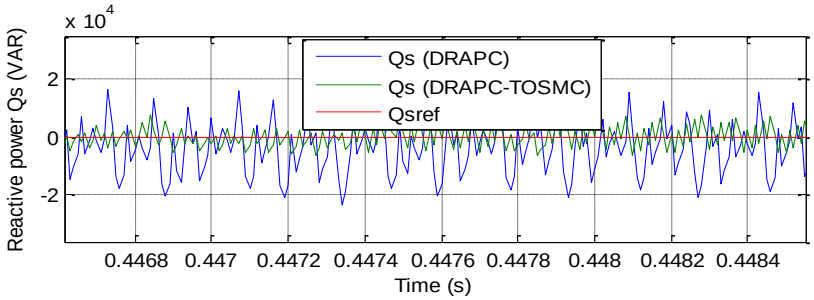

Fig. 24. *Zoom in the reactive power.*

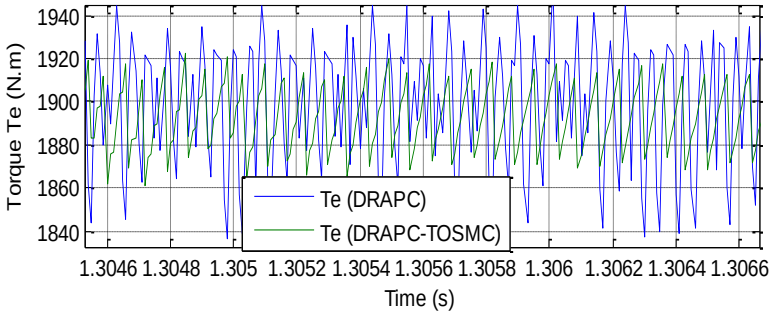

Fig. 25. *Zoom in the electromagnetic torque.*

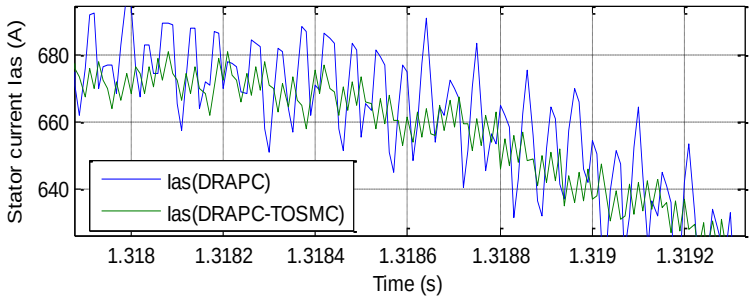

Fig. 26. *Zoom in the current.*

CONCLUSION

To precisely regulate the active and reactive powers of the DFIG in DRWT systems, the novel TOSMC regulators based DRAPC method was proposed in this work. The proposed TOSMC controller was used to command the reactive and active powers and reduce power error. Also, based on the different tests, different objectives were considered. To study the proposed strategy performance, extensive simulations were performed under different wind speeds and the results were compared with those of a lookup table. By implementing the proposed controller, the reference tracking error and power ripples were decreased and the oscillations of the active and reactive powers was damped after disturbance clearance in a faster rate.

REFERENCES

[1] Shehata, E. G. (2015): Sliding mode direct power control of RSC for DFIGs driven by variable speed wind turbines. Alexandria Engineering Journal 54: 1067-1075.

[2] Habib, B. (2017): Hybrid neural sliding mode control of a DFIG speed in wind turbines. Majlesi Journal of Energy Management 6(4): 31-41.

[3] Utkin, V. I. (1993):Sliding mode control design principles and applications to electric drives. IEEE Trans. Ind. Electron. 40(1): 23-36.

[4] Benbouhenni, H. (2019): Sliding mode with neural network regulateur for DFIG using two-level NPWM strategy. Iranian Journal of Electrical & Electronic Engineering 15(3): 411-419.

[5] Benbouhenni, H. (2019): A comparative study between FSMC and FSOSMC strategy for a DFIG-based wind turbine system. MJMS Journal 8(2): 7-14.

[6] Benbouhenni, H. (2020): ANFIS-sliding mode control of a DFIG supplied by a two-level SVPWM technique for wind energy conversion system. International Journal of Applied Power Engineering 9(1): 36-47.

[7] Benbouhenni, H., et al. (2019): Higher control scheme using neural second order sliding mode and ANFIS-SVM strategy for a DFIG-based wind turbine. International Journal of Advances in Telecommunications, Electrotechnics, Signals and Systems 8(2): 17-28.

[8] Gonzales, T., et al. (2012): Variable gain super-twisting sliding mode control. IEEE Transactions on Automatic Control 57(8): 2100-2105.

[9] Yaichi, I., et al. (2019): Super-twisting sliding mode control of a doubly-fed induction generator based on the SVM strategy. Periodica Polytechnica Electrical Engineering and Computer Science 63(3): 178–190.

[10] Benbouhenni, H. (2018): Fuzzy second order sliding mode controller based on three-level fuzzy space vector modulation of a DFIG for wind energy conversion systems. MJMS Journal 7(3):17-26.

[11] Benbouhenni, H. (2018): A comparative study between DTC-NSTMC and DTC-FSTSMC control scheme for a DFIG-based wind turbine. MJEM Journal 7(4).

[12] Benbouhenni, H. (2019): Stator current and rotor flux ripples reduction of DTC DFIG drive using FSTSMC algorithm. International Journal of Smart Grid 3(4).

[13] Benbouhenni, H. (2018): New hybrid five-level space vector modulation strategy to minimize current distortion and power ripple for a DFIG controlled by NSOSMC control. Majlesi Journal of Energy Management 7(2).

[14] Listwan, J. (2018): Application of super-twisting sliding mode controllers in direct field-oriented control system of six-phase induction motor: experimental studies. Power Electronics and Drives 38(3).

[15] Benbouhenni, H., et al. (2020): DPC based on ANFIS super-twisting sliding mode algorithm of a doubly-fed induction generator for wind energy system. Journal Européen des Systèmes Automatisés 53(1): 69-80.

[16] Boudjema, Z., et al. (2017): A novel direct torque control using second order continuous sliding mode of a doubly fed induction generator for a wind energy conversion system. Turkish Journal of Electrical Engineering & Computer Sciences 25(6): 965-975.

[17] Benbouhenni, H. (2018): Rotor flux and torque ripples minimization for direct torque control of DFIG by NSTSM algorithm. Majlesi Journal of Energy Management 7(3).
[18] Benbouhenni, H. (2019): Stator current and rotor flux ripples reduction of DTC DFIG drive using FSTSMC algorithm. International Journal of Smart Grid 3(4).
[19] Benbouhenni, H. (2020): Utilization of an ANFIS-STSM algorithm to minimize total harmonic distortion. International Journal of Smart Grid 4(2): 56-67.
[20] Yahdou, A., et al. (2016): Second order sliding mode control of a dual-rotor wind turbine system by employing a matrix converter. Journal of Electrical Engineering 16(3):1-11.
[21] Yahdou, A., et al. (2015): Sliding mode control of dual rotor wind turbine system. The Mediterranean Journal of Measurement and Control 11(2): 412-419.
[22] Yahdou, A., et al. (2020): Improved vector control of a counter-rotating wind turbine system using adaptive backstepping sliding mode. Journal Européen des Systèmes Automatisés 53(5): 645-651.
[23] Xu, L., et al. (2006): Direct active and reactive power control of DFIG for wind energy generation. IEEE Trans. Energy Convers. 21(3): 750-758.
[24] Mohsen G., Babak M., Soodabeh S. (2014) : A Comparative Study for Rotor Side Converter Controller of a DFIG-Based Wind Turbine, Using Direct Power Control, Carrier-Based PWM Voltage Control and Hysteresis Current Control Strategies. International Journal of Natural and Engineering Sciences 8 (1): 32-41.
[25] Benbouhenni, H. (2019): Stator active and reactive power ripples minimization for DVC control of DFIG by using five-level neural space vector modulation. Acta Electrotechnica et Informatica 19(2):16-23.